Disorder–order structural transition in amorphous LaSrMnO films

2007 J. Phys.: Condens. Matter 19 196218

(http://iopscience.iop.org/0953-8984/19/19/196218)

IOP PUBLISHING JOURNAL OF PHYSICS: CONDENSED MATTER

J. Phys.: Condens. Matter **19** (2007) 196218 (11pp) doi:10.1088/0953-8984/19/19/196218

Disorder–order structural transition in amorphous LaSrMnO films

Z A Samoilenko[1], V D Okunev[1], E I Pushenko[1], N N Pafomov[1], R Szymczak[2], H Szymczak[2] and S J Lewandowski[2]

[1] Donetsk Physico-Technical Institute, Ukrainian Academy of Sciences, 83114 Donetsk, Ukraine
[2] Institute of Physics, Polish Academy of Sciences, Aleja Lotnikow 32/46, 02-668 Warsaw, Poland

E-mail: okunev@mail.fti.ac.donetsk.ua

Received 8 February 2007, in final form 18 March 2007
Published 19 April 2007
Online at stacks.iop.org/JPhysCM/19/196218

Abstract

Using the x-ray diffraction method, the atomic rearrangement in amorphous $La_{0.6}Sr_{0.2}Mn_{1.2}O_3$ films is investigated at growth temperatures $T_s = 20$–$300\,^{\circ}C$. Two stages in the disorder–order phase transition are discovered. In the first stage, amorphous structure undergoes ordering at $T_s = 100\,^{\circ}C$ up to a maximal concentration of small ($D \approx 30$ Å) clusters which occupy 90% of the total volume. In the $T_s = 100$–$150\,^{\circ}C$ temperature interval, disordering in the structure and a change in short-range order prepare the onset of a second stage. In the second stage, starting with $T_s = 150\,^{\circ}C$, the progressive crystallization and transition from mesoscale order to long-range atomic order at $T_s = 300\,^{\circ}C$ take place. It is shown that all transitions produce changes in the conductivity mechanisms and magnetic properties of the films.

1. Introduction

It is well known that the properties of manganites with single-crystal structures are sensitive to changes in their atomic order [1–4]. For systems with disordered structure which can form multiple atomic order [5], such information is absent. At the same time, it is clear that during transition from mesoscopic order to long-range order, one would expect the appearance of new phenomena caused by a change in the scale of atomic ordering.

We investigated the processes of atomic ordering in amorphous LaSrMnO films starting from the disordered state to the long-range order. This was realized by a change in the growth temperature (T_s) of the films from $T_s = 20$ to $300\,^{\circ}C$. It is shown that a rise in T_s results in a non-monotonic character of structural changes caused by the disorder–order phase transition.

2. Samples and experiment

Amorphous LaSrMnO films 0.3–2.5 μm thick were grown by cathodic (dc) sputtering of a $La_{0.6}Sr_{0.2}Mn_{1.2}O_3$ target in an oxygen atmosphere at growth temperatures T_s varying between

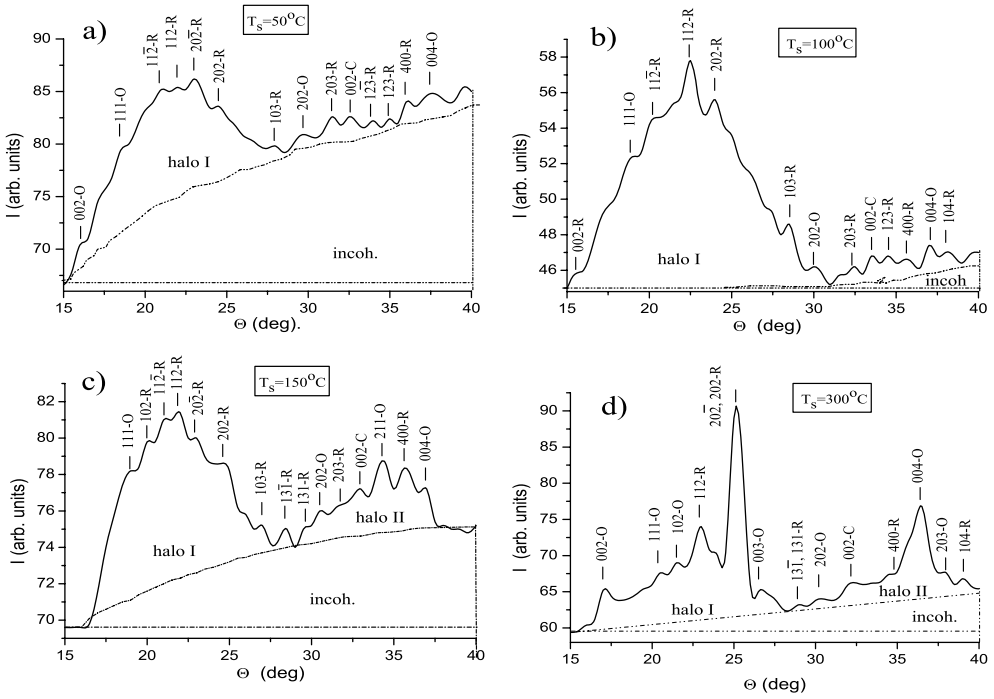

Figure 1. X-ray patterns for LaSrMnO films in which all four structural groups are shown.

20 and 300 °C. A non-stoichiometric composition promotes clustering of the films [5]. Features in x-ray scattering were studied using long-wave Cr Kα radiation [6]. Measurements of magnetization, using a commercial SQUID magnetometer, were carried out over the 4.2–300 K temperature range. Transport measurements were performed in the 80–300 K range.

3. Experimental results and discussion

3.1. Structure: first view

X-ray patterns peculiar to different structural states of amorphous LaSrMnO films are shown in figure 1. Taking into account the characteristic properties of x-ray scattering [3, 6–8], it can be seen that x-ray patterns testify to the presence of three or four structural groups differing in scale:

(i) Medium, with disorderly placed atoms that have short-range order only. This is shown as incoherent scattering with an intensity I_{incoh} increasing as $\sin^2 \Theta$, where Θ is a scattering angle.
(ii) Small, $D = 20$–30 Å in size, mesoscopic groupings of atoms, the so-called amorphous clusters. These form halo1 and halo 2.
(iii) Mesoscopic groupings of average size $D = 100$–200 Å, the so-called crystalline clusters. These form the fluctuations in intensity above the halo.
(iv) Large groupings, $D = 300$–800 Å in size, which are already small crystals with long-range atomic order. These are shown as Debye lines above the halo.

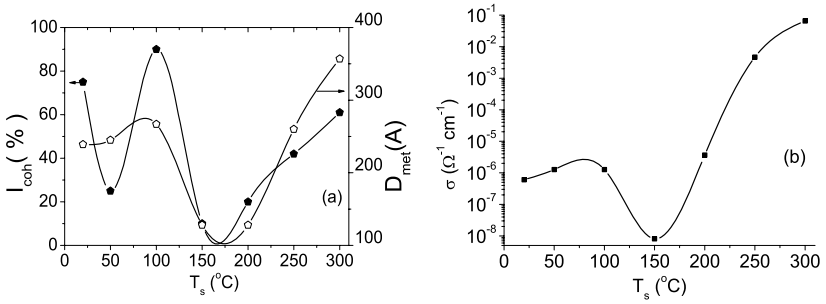

Figure 2. (a) X-ray intensity of coherent scattering by amorphous and crystalline clusters ($I_{coh} = I_a + I_c$) and size of 'metallic' clusters (D_{met}) versus growth temperature (T_s) for LaSrMnO films; (b) conductivity (σ) versus T_s.

3.2. Clusterization and size of clusters

Under an increase in growth temperature from 20 °C up to 150 °C, a maximum in the intensity of coherent scattering equal to 90% of the summed intensity ($\Sigma I = I_{coh} + I_{incoh}$) is observed at $T_s = 100$ °C (figures 1, 2(a)). This related to x-ray scattering by mesoscopic amorphous and crystalline clusters. Simultaneously, the intensity of incoherent scattering by an intercluster disordered medium falls to 10% of the summed intensity (figures 1(a) and (b)). Thus, we observe an increase in the ratio I_{coh}/I_{incoh} from 1/3 at $T_s = 50$ °C to 9 at $T_s = 100$ °C (figure 2(a)). A further increase in the growth temperature up to 150 °C results in a decrease in the I_{coh}/I_{incoh} ratio to 1/9. On the basis of such gigantic changes in the structural parameters of the samples, we have to assume that, in the amorphous state, a phase transition of the disorder–order type is realized in the vicinity of $T_s = 100$ °C. During this transition, a great number of small ($D = 20$–50 Å) groupings of atoms (amorphous clusters) are formed. In figure 1(b) this is seen as an increase in the intensity of halo 1 at a significant decrease in the background caused by incoherent scattering of Cr Kα-radiation. Without taking into account the type of clusters and their conductivity value, the average intercluster distance L can be found using the formula [4]:

$$L = D[(3C)^{-\frac{1}{3}} - 1], \tag{1}$$

where D is the cluster size and C is their concentration. For a sample with $T_s = 100$ °C for which $D = 30$ Å and $C = 0.9$, calculation gives $L = (1$–$2)$ Å, which is equal to the inter-atomic distance. The result that is obtained demonstrates that, in comparison with other samples, at $T_s = 100$ °C the structure is filled to the maximum by clusters. Such a structure should have the maximal density. Experimental evidence for an increase in density under local ordering in amorphous samples is described in [8].

The calculation of cluster sizes (D) with Mn–O bonds of cubic and orthorhombic phases, which can exhibit metallic properties [4], has shown that 'metallic' clusters of maximum size ($D \sim 250$–300 Å) grow at $T_s = 100$ °C (figure 2(a)). Increasing the growth temperature up to $T_s = 150$ °C decreases the cluster size to 100 Å. A further increase in the cluster size is observed at $T_s > 200$ °C (figure 2(a)) caused by a transition from mesoscopic order to long-range atomic order during formation of the crystaline phase in an amorphous medium. Simultaneously, an increase in the intensity of coherent scattering is observed (figure 2(a)). A change in the conductivity of LaSrMnO films grown at different T_s (figure 2(b)) correlates well with the change in size of 'metallic' clusters and the intensity of coherent scattering (figure 2(a)).

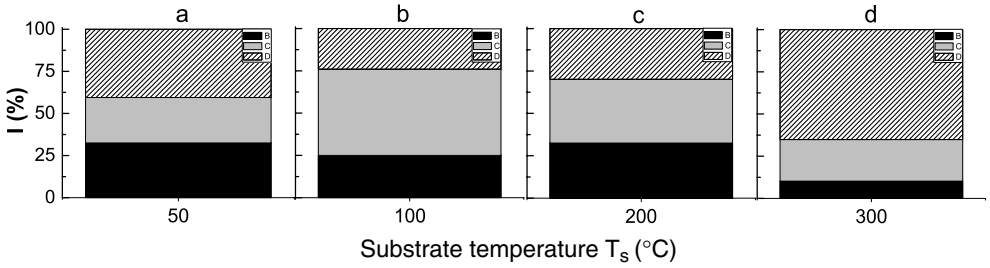

Figure 3. Chart images of relative x-ray intensities scattered by clusters with various manganese charge states for films grown at different temperatures (T_s): (a) 50 °C; (b) 100 °C; (c) 200 °C; (d) 300 °C; (B) area in black for $\Theta = 30°$–$32.5°$ involves $Mn^{(2-3)+}$ states; (C) area in grey for $\Theta = 32°, 5°$–$35°$ involves Mn^{3+} states; (D) shaded area for $\Theta = 35°$–$38°$ involves $Mn^{(3-4)+}$ states.

3.3. Phase composition of 'metallic' clusters

To analyse the diffusive maxima originating from the scattering of Cr Kα-radiation by crystalline clusters with Mn–O bonds, the angular region of $\Theta = 30°$–$38°$ corresponding to halo 2 was divided into three areas: $\Theta_B = 30°$–$32.5°$; $\Theta_C = 32.5°$–$35°$; and $\Theta_D = 35°$–$38°$. These areas differ in interplane distances, charge states of manganese, Mn–O bond lengths, and types of phases [1, 2, 4, 5, 9]. Diagrams of the integral intensity distributions in the indicated intervals of angles θ are represented in figure 3. As can be seen from figure 3(b), for the disorder–order phase transition at $T_s = 100$ °C, the state corresponding to the cubic phase (C) containing trivalent manganese Mn^{3+} prevails in the structure.

Displacing the growth point from $T_s = 100$ °C both to lower ($T_s = 50$ °C, figure 3(a)) or higher ($T_s = 200$ °C, figure 3(c)), we can see that the structure has an approximately equal contribution of three structural states. These are characterized by clusters containing fragments of the following planes: (202) of orthorhombic phase and (203) of rhombohedral phase with the low charge states of manganese, i.e. $Mn^{(2-3)+}$ (area B); (200) of cubic phase including trivalent manganese Mn^{3+} (area C); (400) of rhombohedral phase and (004) of orthorhombic phase with the high charge states of manganese, i.e. $Mn^{(3-4)+}$ (area D). However, during crystallization at $T_s = 300$ °C, the evolution of long-range atomic order enlarges the area D presented mainly by the orthorhombic phase containing $Mn^{(3-4)+}$ ions (figure 3(d)). In contrast, the ordered amorphous state realized at $T_s = 100$ °C has a maximal concentration of Mn^{3+} ions (figure 3(b)).

3.4. Structure and electrical activity of strontium

It is known that for stoichiometric compositions of $LaMnO_3$, all manganese ions have Mn^{3+} charge states. Substitution of Sr^{2+} ions for La^{3+} ions produces the formation of Mn^{4+} ions [1, 2]. According to figure 3, within the limits of amorphous phase existence, the concentration of Mn^{4+} ions varies noticeably, which characterizes a change in the electrical activity of strontium. In the process of atomic ordering at $T_s = 100$ °C, the activity of strontium is minimal, which corresponds to the classical behaviour of an impurity in amorphous and glassy semiconductors [10], when all impurity atoms saturate their valent bonds and form closed electronic configurations, creating neither acceptor nor donor states. The behaviour of strontium is one of the indications of a difference in the short-range orders of the amorphous and crystaline states of LaSrMnO (figures 3(b) and (d)).

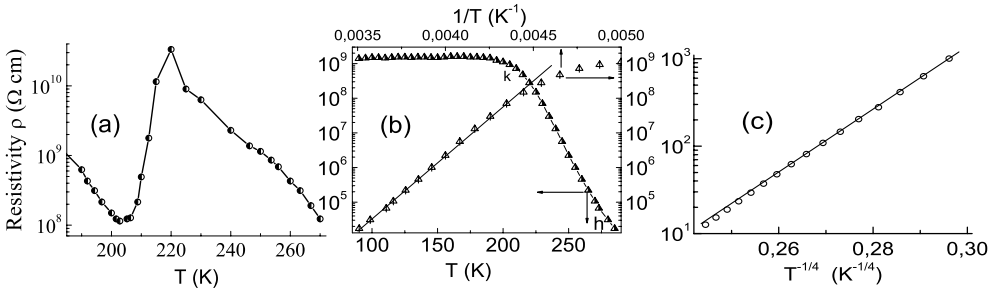

Figure 4. Typical temperature dependences of resistivity for amorphous LaSrMnO films with 'metallic' clusters of different sizes D: (a) D = 60–100 Å; (b) D = 30–60 Å; (c) for films containing crystals of small size, D = 200–500 Å.

In manganese oxides such as $La_{1-x}Sr_x(Ca)MnO_3$, manganese ions with different charge states, i.e. Mn^{2+}, Mn^{3+}, and Mn^{4+}, can coexist [1]. The reason for the appearence of Mn^{2+} ions consists of the presence of local stresses stimulating the reaction $2Mn^{3+} \rightarrow Mn^{2+}+Mn^{4+}$. It is obvious that maximal stresses are realized in the films grown at low temperatures. Indeed, for films grown at $T_s \leqslant 200\,^{\circ}C$, an appreciable concentration of structural groups containing Mn^{2+} ions is observed as area B in figures 3(a)–(c). The evident tendency to decrease in stress under an increase in T_s resulted in a narrowing of area B, which is minimal at $T_s = 300\,^{\circ}C$ (figure 3(d)).

3.5. Mechanisms of electrical conductivity

Evolution of the atomic order and cluster structure of samples differing in growth temperature agrees with the changes in electrical and magnetic properties. In the amorphous state (T_s = 20–200 °C), the films are insulators, with resistivity at room temperature changing from $\rho = 2 \times 10^5$ Ω cm to 1×10^8 Ω cm. Before the formation of crystal structure, the electrical properties of the samples are limited by the tunnelling of charge carriers between clusters with metallic conductivity [4, 5]. Generally, the conductivity of the samples containing 'metallic' clusters is given by the equation $\rho \approx \rho_0 \exp(A/T)$ [11, 12], where $\rho_0 \approx \rho_{min} \exp(L/l)$. Here l is the tunnelling length, L is the intercluster distance, A is a constant, and $\rho_{min} = 1/\sigma_{min}$, where σ_{min} is the value of the minimum metallic conductivity [13]. For amorphous films containing a small quantity of metallic clusters, the condition of strong localization is satisfied, $L/l > A/T$ [11], and specific parameters of the cluster structure (type of packing, size of clusters, and their concentration) affect the form of the $\rho(T)$ curve mainly at low temperatures.

Maximum resistivity is realized in the films grown at $T_s = 150\,^{\circ}C$ (figure 4(a)) having the maximum disordered structure. These films contain small clusters ($D \approx 110$ Å) with metallic conductivity and large volume, ∼90% of the total volume, of the disordered intercluster medium.

At $T_s = 100\,^{\circ}C$, the disorder–order structural transition produces an increase in the concentration of small ($D \sim$ 20–30 Å) amorphous clusters and a decrease in the volume of the intercluster medium with disorderly located atoms (figure 1). Therefore, the resistivity value of the film grown at $T_s = 100\,^{\circ}C$ is 2.5 orders of magnitude lower than that of the sample grown at $T_s = 150\,^{\circ}C$, at which processes of disordering prevail and the total intensity of coherent scattering by amorphous and crystalline clusters ($I_a + I_c$) is minimal (figure 2(a)). In the T_s = 20–100 °C temperature interval, the conductivity as well as the sizes of metallic clusters increase slightly with an increase in the growth temperature (figures 2(a) and (b)).

In the case of $D > 20$ Å, the clusters can show metallic properties [5]. There are three kinds of temperature dependences of resistivity for amorphous films differing in the size of 'metallic' clusters (figure 4). If $D = 60$–100 Å, as well as for crystals, $\rho(T)$ curves have a section with a maximum, a minimum, and gigantic derivative values of $\mathrm{d}\rho/\mathrm{d}T > 10^4\%\ \mathrm{K}^{-1}$ (figure 4(a)). For crystals, $\mathrm{d}\rho/\mathrm{d}T = 1$–$8\%\ \mathrm{K}^{-1}$ [4] and can reach 25–30% K^{-1} [14]. According to the results reported in [15], it is possible to explain the presence of a minimum for the $\rho(T)$ curves through the energy minimum of a cluster system (E_{drop}) with metallic conductivity (metallic droplets) inside an insulator matrix. In fact, if the energy of Coulomb interaction of free charge carriers into the cluster is low, this will be seen qualitatively from the equation for E_{drop} obtained in [15], writing this equation in a simplified form: $E_{\mathrm{drop}} \approx -An_{\mathrm{drop}}(T)\{B - C/[D(T)]^2\} - G\{1 - Fn_{\mathrm{drop}}(T)[D(T)]^3\}$, where n_{drop} is the concentration of metallic clusters (droplets), D is the cluster size, and A, B, C, G, and F are constants. We assume that n_{drop} and D are functions of temperature. The $D(T)$ dependence is evident [12], and the temperature dependence of n_{drop} is related to the existence of a critical size of a 'metallic' cluster equal to double the thickness h of the depletion layer [16], $h = (2\varepsilon\varepsilon_0 V_D/ep)^{1/2}$, where ε is the static dielectric constant of the material, ε_0 is the permittivity of vacuum, V_{D} is the diffusion potential, e is the electron charge, and p is the hole concentration. The value of $(2h)_{\mathrm{crit}}$ for LaSrMnO is equal to 20 Å [4].

In the films with $D = 30$–60 Å, the capture of holes by localized states in peripheral areas of clusters occurs. As a result, the concentration of free holes decreases, and quantum confinement effects become apparent. If the temperature goes down, the requirement $\delta E = (D^3 N(E_{\mathrm{F}})P^{-1}) \geqslant kT$ can be satisfied. Here $N(E_{\mathrm{F}})$ is the density of states at the Fermi level, and δE is the separation energy between quantum confinement levels. In this case, the clusters lose their metallic properties and transform into a system of tunnelling-coupled quantum dots [5] which have a typical section $\rho(T) = \mathrm{const}$ on the $\rho(T)$ curves (figure 4(b)).

In the high-temperature region, the temperature dependence of resistivity is determined by the Coulomb interaction of charge carriers on tunnelling between metallic clusters [12, 17] and is given by the equation $\rho(T) = \rho_0 \exp(W_{\mathrm{D}}/kT)$, where k is the Boltzmann constant, $W_D \approx e^2/\varepsilon D[1 - (C_{\mathrm{m}}/C_{\mathrm{m}}^{\mathrm{crit}})^{1/3}]$ is the charging energy, which is dependent on the cluster size D, e is the electronic charge, ε is the permittivity, and $C_{\mathrm{m}}^{\mathrm{crit}}$ corresponds to a percolation threshold. For section kh of the $\rho(T)$ curve plotted in the coordinates $\log(\rho) - 1/T$ (figure 4(b)), the activation energy $W_D = 0.86$ eV corresponds to a spherical cluster size of $D = 15$ Å. Taking into account that clusters are quasi-two-dimensional formations of thickness $h \sim D/3$ [3], we obtain a size of flat clusters equal to $35 \times 35 \times 11$ Å at identical volumes. These values coordinate well with x-ray data. The anisotropic shape of the nanoscale ferromagnetic droplets in the magnetics is energetically more favourable [18]. A decrease in resistivity from $\rho = 10^{10}\ \Omega$ cm to $10^1\ \Omega$ cm occurs on a change in the conductivity mechanism from tunnel type, realized due to the participation of metallic clusters (figure 4(a) and (b)), to a variable range hopping described by Mott's law [10]: $\rho(T) = \rho_0 \exp[(T_0/T)^{1/4}]$ (figure 4(c)). According to the x-ray data (figure 1), these changes are caused by the transition from mesoscopic order to long-range atomic order, from the amorphous state of the structure to the crystalline state. Thus, impurity atoms of strontium become electrically active, creating Mn^{4+} ions directly in the structure of solid solution [5] (figure 3(d)). The Mn^{3+} and Mn^{4+} ions take part in variable range hopping according to the standard scheme $\mathrm{Mn}^{3+} + \mathrm{Mn}^{4+} \rightarrow \mathrm{Mn}^{4+} + \mathrm{Mn}^{3+}$ (figure 4(c)) peculiar to the materials containing electronic states overlapping in energy for ions of different valence states. For the samples under investigation, the experimental $\rho(T)$ curves come into agreement with Mott's law at $T < 240$ K.

Independently of the form of the $\rho(T)$ curves (figure 4) and the mechanisms of conductivity at low temperatures, the resistivity of the films measured at room temperature

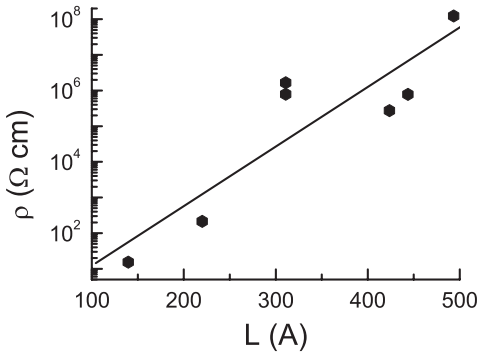

Figure 5. Room-temperature resistivity versus distance between 'metallic' clusters in LaSrMnO films.

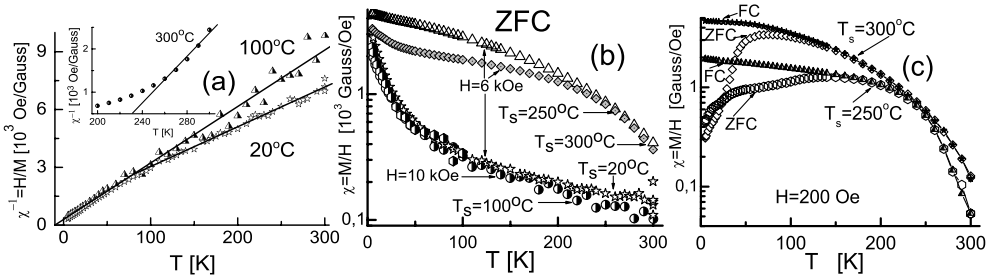

Figure 6. Magnetic susceptibility versus temperature for LaSrMnO films grown at different T_s.

is limited by the tunnelling of electrons between metallic clusters, dependent exponentially on the intercluster distance. Therefore, we can compare results of the change in resistivity for the whole interval. In accordance with expectation, resistivity increases exponentially with an increase in distance (L) between clusters: $\rho = \rho_0 \exp(L/L_0)$, where L is calculated by means of formula (1) for medium-sized metallic clusters of $D_{\text{met}} = 200$ Å and taking into account the individual concentration values of metallic phase appreciated by means of the intensities of corresponding diffusive maxima (figure 5). Calculation of the intercluster distances on the basis of x-ray data does not guarantee the inclusion of clusters with metallic conductivity only. Moreover, formula (1) does not take into account specific features of the shape, sizes and spatial distribution of the clusters. We believe that these facts serve as main reasons for the wide dispersion in resistivity values in figure 5. In particular, this is shown in the high value of $\rho_o \approx 1 \times 10^{-1}$ Ω cm estimated from the data in figure 5 at $L = 0$. For a coordination number $z = 6$, the corresponding minimum in metallic conductivity (σ_{min}) should be $3 \times 10^2\ \Omega^{-1}\text{cm}^{-1}$ [13]. We are of the opinion that the value of $\sigma_o = 1/\rho_o \approx 10\ \Omega^{-1}\ \text{cm}^{-1} \ll 3 \times 10^2\ \Omega^{-1}\ \text{cm}^{-1}$ is caused by the overstated concentrations of the metallic phase in the samples.

3.6. Change in the mechanism of magnetic interaction

The beginning of crystallization and generation of Mn^{4+} ions in the samples causes the onset of the phase transition from the paramagnetic state (the bottom curves in figure 6(b)) to the ferromagnetic state (figure 6(c) and the top curves in figure 6(b)) when small ferromagnetic crystals grow in a paramagnetic medium. This testifies to the change in short-range order,

since it is well known that magnetic interactions have a high sensitivity to rearrangement in the environment nearest to magnetic ions.

For paramagnetic samples grown at low T_s, one can approximate the experimental data using the Curie–Weiss law:

$$\chi(T) = M/H = B + \frac{C}{T - \Theta_p}, \tag{2}$$

where M is the magnetization, H is the magnetic field, and Θ_p is the Weiss constant or paramagnetic Curie temperature. For a sample grown at $T_s = 100\,^{\circ}\mathrm{C}$ and measured at $H = 10$ kOe, we can write $\chi(\mathrm{Gs\ Oe^{-1}}) = 3.4 \times 10^{-5} + 2.98 \times 10^{-2}/(T + 7.48)$. Similarly, data for a sample grown at $T_s = 20\,^{\circ}\mathrm{C}$ follow the equation $\chi(\mathrm{Gs\ Oe^{-1}}) = 4.05 \times 10^{-5} + 3.12 \times 10^{-2}/(T + 5.045)$. We have to pay attention to the sign (+) enclosed in the round brackets, indicating the negative Θ_p value that exhibits the tendency to antiparallel orientation of the magnetic moments under an external field. The increase in the Θ_p value from 5.045 to 7.48 K with T_s changing from 20 to 100 °C can characterize the strengthening of the antiferromagnetic interactions in the paramagnetic medium of the samples grown at $T_s = 100\,^{\circ}\mathrm{C}$ and containing the highest concentration, ∼90% of the total volume, of small clusters in the structure. These clusters form the first halo (figure 1), intensifying it sharply at $T_s = 100\,^{\circ}\mathrm{C}$ (figure 1(b)). Thus, we can suggest that before crystallization, an amorphous medium has a weak tendency to antiferromagnetic ordering. This assumption agrees well with the results reported earlier [5], which give evidence for the absence of electrical activity in strontium in the amorphous state of the films and show a similarity to local atomic order peculiar to antiferromagnetic $SrMnO_3$. In the amorphous state, the magnetic moments of small ferromagnetic clusters are weak, randomly oriented, and therefore the total magnetization has a paramagnetic character determined by the external field. However, it is interesting to make a brief comparison of the results with a simple theory for the magnetic susceptibility, (χ), of manganites containing metallic clusters inside an insulating intercluster medium [19]. The coexistence of the different magnetic phases is a distinctive feature for manganites [1, 2, 7, 20]. According to the results of [19], it is possible to observe an effect of ordering in the system of ferromagnetic clusters on the $\chi(T)$ dependence at low or moderate concentrations of the clusters.

In figure 6(a), $\chi^{-1}(T)$ curves are shown for films grown at temperatures $T_s = 20$, 100 and 300 °C containing, according to x-ray data, 2%, 1.4%, and 7.8% of ferromagnetic clusters, respectively. Evidently, for a sample with $T_s = 100\,^{\circ}\mathrm{C}$ containing 3×10^{15} cm^{-3} ferromagnetic clusters of size $D = 250$ Å, the intercluster distance $L = 450$ Å is too large to have an influence on the $\chi^{-1}(T)$ dependence (straight line named '100 °C' in figure 6(a)). However, in samples grown at $T_s = 20\,^{\circ}\mathrm{C}$, the increase in the concentration of clusters up to 1×10^{16} cm^{-3} on a simultaneous decrease in their size to $D = 200$ Å decreases the intercluster distance to $L = 300$ Å and strengthens, in that way, the interaction between clusters, resulting in the appearance of the $\chi^{-1}(T)$ dependence as two broken lines (named '20 °C' in figure 6(a)). The sensitivity threshold of the $\chi(T)$ curves to the concentration of ferromagnetic clusters is in agreement with a prediction of the theory [19]. For films grown at $T_s = 300\,^{\circ}\mathrm{C}$ which contain 6.5×10^{17} cm^{-3} ferromagnetic clusters, the parameters of the cluster structure ($C_m = 7.8\%$, $D = 180$ Å, and $L = 100$ Å) are sufficient for appreciable interaction between them. For this case, the $\chi^{-1}(T)$ curve named '300 °C' (insert in figure 6(a)) has a behaviour that is well discussed in [19].

For films grown at $T_s = 250$–$300\,^{\circ}\mathrm{C}$, i.e. at the initial stage of crystallization, the temperature dependence of the magnetic susceptibility, $\chi(T)$, is fundamentally different compared to that of samples grown at lower T_s (figure 6(b)). So, the upper curves in figure 6(b) show the presence of a ferromagnetic phase. Ferromagnetic interactions become apparent best

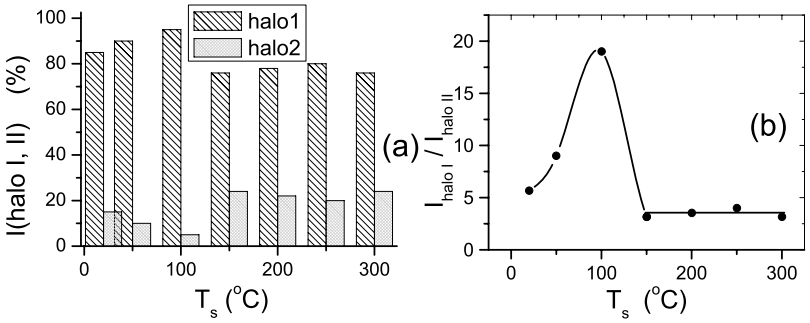

Figure 7. Intensities of halo 1 and halo 2 (a) and their ratio (b) versus growth temperature T_s for LaSrMnO films.

of all in the difference in the $\chi(T)$ curves measured in low magnetic fields under the ZFC (zero field cooling) or FC (cooling in the presence of a magnetic field) regimes, as is shown in figure 6(c). These results come to an agreement with the data of electrical measurements, showing a sharp increase in the electrical activity of strontium atoms at the initial stage of crystallization when formation of the Mn^{3+} and Mn^{4+} electronic states overlapping in energy is observed in the $LaMnO_3$–$SrMnO_3$ solid solution.

3.7. Two stages of phase transition

The reported results allow us to believe that, in the amorphous state of LaSrMnO films, two groups of clusters are formed. These have different atomic orders and become apparent in two halos on the diffraction patterns (figure 1), as was observed earlier for amorphous multicomponent materials [21]. Examining each growth temperature (T_s) as a defined point of atomic order, let us consider the evolution of the structure for the polyatomic LaSrMnO system under an increase in T_s. An increase in T_s from 20 to 100 °C stimulates the preferred growth of structural fragments in the form of the dense (112) planes of rhombohedral phase represented in halo 1 in figure 1(b). At the same time, fragments of the Mn–O planes as groups of planes of cubic, rhombohedral and orthorhombic phases form halo 2. For the samples grown at T_s = 20–100 °C, the intensity of halo 1 increases and that of halo 2 decreases (figure 7(a)). This difference is especially distinctive in the ratio of the intensities of halo 1 and halo 2, which has a maximum at T_s = 100 °C (figure 7(b)).

Under an increase in growth temperature from T_s = 100 °C to T_s = 150 °C, the intensity of x-ray scattering by the second group of structural elements containing Mn–O bonds that form halo 2 increases appreciably for a decrease in the contribution of the first group presented by halo 1 to the total intensity (figure 7(a)). At the coincidence of the short-range atomic orders for the amorphous and crystalline states, we should have monotonous changes in all the parameters for an increase in T_s. However, because of the different environments around strontium and manganese atoms at $T_s \leqslant 100$ °C and at $T_s \geqslant 150$ °C, the state formed at T_s = 100 °C is unstable, and the short-range order is rearranged under the change in growth temperature from 100 to 150 °C. At the same time, the intensity of x-ray scattering by the second structural group to form halo 2 increases and that of the first group in the form of halo 1 decreases (figure 7(a)). As a result, the ratio of their intensities falls sharply from 19 to 3.3 (figure 7(b)). Starting from 150 °C, a further increase in T_s does not give a change in the relative intensities of halo 1 and halo 2 (figures 7(a) and (b)). Such constancy in the relative intensity of reflections at x-ray scattering is typical for crystal structures only and shows that, in the interval T_s = 150–300 °C,

the short-range order is not changed any more. Here, a disorder–order phase transition is shown as an increase in the cluster sizes on transition from mesoscale order to long-range atomic order. Changes in the atomic order for mesoscale areas have been observed earlier for phase transitions in a PbLaTiZr solid solution [22, 23]. Hence, the disorder–order phase transition in amorphous LaSrMnO films consists of two stages of changes in the atomic structure. In the first stage, an intermediate minimum in free energy characteristic of a metastable state is formed. In this state, 90% of the volume of the film grown at $T_s = 100\,^{\circ}\mathrm{C}$ is occupied by small clusters. Next, the short-range atomic order undergoes a reconstruction, and a stable short-range order peculiar to the basic minimum in free energy of the crystalline LaSrMnO system is formed, starting from $T_s = 150\,^{\circ}\mathrm{C}$, i.e. in an amorphous state of the structure.

The changes in atomic order correlate well with the results of electrical and magnetic measurements. So, the samples grown at $T_s = 100\,^{\circ}\mathrm{C}$ have as much as possible a clustered structure and are paramagnetic, with electrical properties typical of insulators. The influence of the second structural group presented by halo 2 on properties of the films is minimal (figure 7(a)).

At $T_s = 250$–$300\,^{\circ}\mathrm{C}$, the strengthening of interatomic interaction in the samples results in the formation of a long-range atomic order (figure 1(d)). Debye lines on halo 1 and halo II testify to this. The appearance of the (004) line of the orthorhombic phase on halo 2 presents evidence for the growth of crystals with ferromagnetic properties (figures 6(b) and (c)). A sharp increase in the electrical activity of strontium atoms during crystallization of the films increases their conductivity in the limit of seven orders of magnitude (figure 2(b)).

4. Conclusions

We have discovered two stages of the disorder–order phase transition in the atomic structure of amorphous LaSrMnO films under an increase in their growth temperature (T_s):

(1) It is shown that, in the first stage, at $T_s = 100\,^{\circ}\mathrm{C}$, small clusters of $D \sim 30$ Å with a minimal distance of $L \sim 1$–2 Å between them are formed at the cost of the disordered intercluster medium.
(2) At $T_s = 150$–$300\,^{\circ}\mathrm{C}$, a second stage of ordering with the formation of a long-range atomic order is observed.
(3) In the $T_s = 100$–$150\,^{\circ}\mathrm{C}$ interval, a change in short range atomic ordering is realized.
(4) At $T_s \geqslant 250\,^{\circ}\mathrm{C}$, the formation of crystalline structure results in a change of the conductivity mechanism from spin-dependent tunnelling between clusters with metallic conductivity to a variable-range hopping, at which Mn^{3+} and Mn^{4+} centres start to play an important role.
(5) In the amorphous state, LaSrMnO films grown at $T_s < 250\,^{\circ}\mathrm{C}$ are paramagnets containing a little of the ferromagnetic and antiferromagnetic clusters. Ferromagnetic behaviour is observed at $T_s \geqslant 250\,^{\circ}\mathrm{C}$, after the beginning of crystallization.

Acknowledgment

This work was partly supported by the Ministry of Science and Higher Education of Poland project PBZ-KBN-115/T08/2004.

References

[1] Coey J M D, Viret M and von Molnar S 1999 *Adv. Phys.* **48** 167
[2] Goodenough J B, Zhou J S, Rivadulla F and Winker E 2003 *J. Solid State Chem.* **175** 116

[3] Okunev V D, Samoilenko Z A, Abal'oshev A, Baran M, Berkowski M, Gierlowski P, Lewandowski S J, Szewczyk A, Szymzak H and Szymczak R 2004 *Phys. Lett.* A **325** 79
[4] Okunev V D, Samoilenko Z A, Pafomov N N, Plehov A L, Szymczak R, Baran M, Szymczak H, Lewandowski S J, Gierowski P and Abal'oshev A 2004 *Phys. Lett.* A **332** 275
[5] Okunev V D, Samoilenko Z A, Pafomov N N, D'yachenko T A, Plehov A L, Szymczak R, Baran M, Szymczak H and Lewandowski S J 2005 *Phys. Lett.* A **346** 232
[6] Okunev V D, Samoilenko Z A, Svistunov V M, Abal'oshev A, Dynowska E, Gierlowski P, Klimov A and Lewandowski S J 1999 *J. Appl. Phys.* **85** 7282
[7] Krivoglaz M A 1988 Electronic theory of heterogeneus states in solids *Elektronnaya Struktura I Elektronnye Svoistwa Metallov i Splavov* (Kiew: Naukova Dumka) (in Russian)
[8] Kitaigorodsky A I 1952 *X-ray Structure Analysis of Fine Crystalline and Amorphous Solids* (Moskva-Leningrad: Gostechizdat) (in Russian)
[9] Okunev V D, Samoilenko Z A, Szymczak R and Lewandowski S J 2005 *Zh. Eksp. Teor. Fiz.* **128** 150
Okunev V D, Samoilenko Z A, Szymczak R and Lewandowski S J 2005 *JETP* **101** 128 (Engl. Transl.)
[10] Mott N F and Devis E A 1979 *Electronic Processes in Non-Crystalline Materials* (Oxford: Oxford University Press)
[11] Rakhmanov A L, Kugel K I, Blanter Ya M and Kagan M Yu 2001 *Phys. Rev.* B **63** 174424
[12] Okunev V D, Szymczak R, Baran M, Szymczak H and Gierłowski P 2006 *Phys. Rev.* B **74** 014404
[13] Mott N F 1990 *Metal–Insulator Transitions* (London: Taylor and Francis)
[14] Daoudi K, Tsuchiya T, Yamaguchi I, Manabe T, Mizuta S and Kumagai T 2005 *J. Appl. Phys.* **98** 013507
[15] Kagan M Yu and Kugel' K I 2001 *Phys.—Usp.* **44** 577
[16] Sze S M 1981 *Physics of Semiconductors* (New York: Wiley)
[17] Helman J S and Abeles B 1976 *Phys. Rev. Lett.* **37** 1429
[18] Kagan M Yu, Kugel K I, Rakhmanov A L and Pazhitnykh K S 2006 *J. Phys.: Condens. Matter* **18** 10905
[19] Kugel K I, Rakhmanov A L, Sboychakov A O, Kagan M Yu, Brodsky I V and Klaptsov A V 2004 *J. Exp. Theor. Phys.* **98** 572
[20] Banerjee A, Pramanik A K, Kumar K and Chaddah P 2006 *J. Phys.: Condens. Matter* **18** L605
[21] Okunev V D and Samoilenko Z A 1986 *JETP Lett.* **43** 28
[22] Ishcuk V M and Sobolev V L 2002 *J. Appl. Phys.* **92** 2086
[23] Ishcuk V M, Baumer V N and Sobolev V L 2005 *J. Phys.: Condens. Matter* **17** L177